HHS Public Access

Author manuscript

*Bone*. Author manuscript; available in PMC 2022 July 01.

Published in final edited form as:

*Bone*. 2021 July ; 148: 115941. doi:10.1016/j.bone.2021.115941.

# Osteolineage Depletion of Mitofusin2 Enhances Cortical Bone Formation in Female Mice

**Allahdad Zarei**[#1], **Anna Ballard**[#1], **Linda Cox**[1], **Peter Bayguinov**[2], **Taylor Harris**[3,4], **Jennifer L. Davis**[1], **Philip Roper**[1], **James Fitzpatrick**[2,4,5], **Roberta Faccio**[3,6], **Deborah J. Veis**[1,6,7]

[1]Musculoskeletal Research Center, Division of Bone and Mineral Disease, Washington University School of Medicine, St. Louis, MO 63110, USA

[2]Washington University Center for Cellular Imaging, Washington University School of Medicine, St. Louis, MO 63110, USA

[3]Department of Orthopedic Surgery, Washington University School of Medicine, St. Louis, MO 63110, USA

[4]Department of Biomedical Engineering, Washington University in St. Louis, St. Louis, MO 63130, USA

[5]Departments of Neuroscience and Cell Biology & Physiology, Washington University School of Medicine, St. Louis, MO 63110, USA

[6]Shriners Hospitals for Children, St. Louis, MO, 63110 USA

[7]Department of Pathology and Immunology, Washington University School of Medicine, St. Louis, MO, 63110 USA

[#] These authors contributed equally to this work.

## Abstract

Mitochondria are essential organelles that form highly complex, interconnected dynamic networks inside cells. The GTPase mitofusin 2 (MFN2) is a highly conserved outer mitochondrial membrane protein involved in the regulation of mitochondrial morphology, which can affect various metabolic and signaling functions. The role of mitochondria in bone formation remains unclear. Since MFN2 levels increase during osteoblast (OB) differentiation, we investigated the role of MFN2 in the osteolineage by crossing mice bearing floxed *Mfn2* alleles with those bearing Prx-cre to generate cohorts of conditional knock out (cKO) animals. By *ex vivo* microCT, cKO female mice, but not males, display an increase in cortical thickness at 8, 18, and 30 weeks, compared to wild-type (WT) littermate controls. However, the cortical anabolic response to

Corresponding author: Deborah J. Veis, dveis@wustl.edu; 660 S. Euclid Ave, Box 8301, St. Louis, MO 63110, USA.

Author contributions

Allahdad Zarei: Investigation, Writing – Original Draft Preparation, Visualization. Anna Ballard: Visualization, Formal analysis, Writing – Original Draft Preparation and Review and Editing. Linda Cox: Investigation. Peter Bayguinov: Investigation. Taylor Comte: Investigation, Visualization, Formal analysis. Jennifer L. Davis: Investigation, Writing – Review and Editing. Philip M Roper: Investigation, Writing – Review and Editing. James Fitzpatrick: Methodology, Supervision. Roberta Faccio: Conceptualization, Writing – Review and Editing. Deborah J. Veis: Conceptualization, Funding acquisition, Writing – Review and Editing.

Competing interests

The authors have no competing interests to declare.

mechanical loading was not different between genotypes. To address how *Mfn2* deficiency affects OB differentiation, bone marrow-derived mesenchymal stromal cells (MSCs) from both wild-type and cKO mice were cultured in osteogenic media with different levels of β-glycerophosphate. cKO MSCs show increased mineralization and expression of multiple markers of OB differentiation only at the lower dose. Interestingly, despite showing the expected mitochondrial rounding and fragmentation due to loss of MFN2, cKO MSCs have an increase in oxygen consumption during the first 7 days of OB differentiation. Thus, in the early phases of osteogenesis, MFN2 restrains oxygen consumption thereby limiting differentiation and cortical bone accrual during homeostasis *in vivo*.

**Keywords**

mitochondria; osteogenesis; osteoblast; bone formation; mitofusin

## 1. Introduction

Osteoblast (OB) differentiation *in vivo* and *in vitro* is dependent on stage-specific variations in the acquisition of energy. While early osteogenic differentiation requires oxidative phosphorylation, cells undergo a metabolic shift to glycolysis during late OB maturation and mineralization [1–3]. In most cell types, the degree to which oxidative phosphorylation or glycolysis predominates is largely influenced by mitochondrial organization and turnover. Termed mitochondrial dynamics, the processes of mitochondrial biogenesis, fission, fusion, and mitophagy are interrelated [4–7]. Increased biogenesis, leading to higher mitochondrial mass, along with fusion, tend to increase oxidative phosphorylation, while fission tends to reduce it. Mitophagy, the selective autophagy of mitochondria, generally removes damaged mitochondria, thereby improving the efficiency of the network. OB differentiation is highly correlated with mitochondrial mass and activity, but little is known about the relationship between OB formation or function and mitochondrial dynamics [8].

A major player in mitochondrial dynamics is mitofusin 2 (MFN2), a transmembrane GTPase on the outer mitochondrial membrane that promotes mitochondrial fusion as well as mitophagy. In humans, mutations in *MFN2* are associated with the neurodegenerative disorder Charcot Marie Tooth Syndrome 2A [9]. While much evidence supports MFN2 importance in neurons, as well as cardiomyocytes, much less is known about this mitochondrial protein in other cell types. In general, MFN2 depletion seems to decrease oxygen consumption with a compensatory increase in glycolysis [10]. Several studies, employing a variety of sources for human and murine mesenchymal stromal cells (MSCs), suggest that *in vitro* osteogenesis leads to upregulation of MFN2 expression and subsequent increases in mitochondrial content and oxygen consumption [11–14]. In the single study directly addressing osteogenesis and MFN2, its depletion in murine skin-derived MSCs decreased oxygen consumption, but surprisingly also extracellular acidification, an indication of glycolysis, early in differentiation [8]. However, because energy metabolism shifts significantly during the course of OB differentiation, with important roles for both oxidative phosphorylation and glycolysis, *in vivo* studies are required to understand the

physiological role of mitochondrial dynamics in this cell type. This prompted us to further explore MFN2 in the OB using a murine model.

Due to its critical role in the regulation of mitochondrial dynamics, we hypothesized that MFN2 is important for osteogenesis and bone formation. To directly target the early phase of osteogenesis, we generated conditional MFN2-deficient mice using Prx-cre. In female mice, we find that lack of MFN2 in the OB lineage is associated with increased basal bone formation *in vivo* and enhanced differentiation with a suboptimal osteogenic stimulus *in vitro*, accompanied by increased oxidative phosphorylation.

## 2. Materials and Methods

### 2.1 Reagents and mice

All chemicals and reagents were purchased from MilliporeSigma (Saint Louis, MO, USA) unless otherwise mentioned. Prx-cre males (Jackson Laboratories, Stock # 005584 [15]) were crossed with *Mfn2*$^{fl/fl}$ females [16], to delete exon 6 of *Mfn2* upon Cre-mediated recombination, thereby generating experimental cohorts of wild-type (WT =*Mfn2*$^{fl/fl}$*; Prx-cre*$^{-/-}$) and cKO (*Mfn2*$^{fl/fl}$*; Prx-cre*$^{+/}$) animals. Mice were housed under standard conditions and all *in vivo* protocols were performed with approval from the Institutional Animal Care and Use Committee at Washington University School of Medicine (ASC protocol # 20170025), in accordance with ARRIVE guidelines.

### 2.2 Cell culture

Mouse bone marrow stromal cells (MSCs) from tibia/femur bone marrow flushes were expanded in growth medium containing Minimum Essential Medium Eagle-Alpha Modifications (α-MEM), containing 10% heat-inactivated fetal bovine serum (HI-FBS), 1X PenStrep, and 2 mM L-glutamine (Gibco, Grand Island, NY, USA) in 150mm tissue culture dishes. At subconfluence, cells were plated in triplicate in osteogenic differentiation media (OSM: 5 or 10 mM β-glycerolphosphate disodium salt (β-GP), as indicated, and 50 μg/ml L-ascorbic acid) at $2x10^5$ in 6 well-plates for gene expression or $1x10^6$ in 100mm dishes for protein expression. The 5 mM dose of β-GP used is suboptimal for osteogenesis in WT cultures.

### 2.3 Real-time RT-PCR

For tissue RNA extraction, epiphyses were removed, marrow flushed, and remaining bone was flash frozen in trizol and crushed. Total RNA from bones and cultured cells was extracted with NucleoSpin RNA kit (Machery-Nagel, Bethlehem, PA, USA) and cDNA synthesis was performed with RNA to cDNA EcoDry™ Premix (Takara Bio, Mountain view, CA, USA). RT-PCR was performed on an ABI QuantStudio 3 Thermal Cycler (Applied Biosystems) using iTaq Universal SYBR Green Supermix (Bio-Rad) for 50°C for 2 m, 95°C for 10 m, and then 40 cycles of 95°C for 15 s and 60 °C for 1 m.Primer sequences are listed in the Resources table.

### 2.4 Western blots

Cell lysates were extracted on ice in RIPA buffer (20mM Tris, pH 7.5, 150mM NaCl, 1mM EDTA, 1mM EGTA, 1% Triton X-100, 2.5 mM sodium pyrophosphate, 1mM β-glycerophosphate, 1mM $Na_3VO4$, 1mM NaF) containing 1:20 HALT protease inhibitor cocktail. Protein concentrations in total lysates were determined by BCA protein assay kit (Bio-Rad Laboratories, Hercules, CA, USA) according to the manufacturer's instructions. Proteins (5-30μg) were fractionated by 10% SDS-PAGE, transferred onto nitrocellulose membranes, blocked in 5% non-fat dry milk-TBST for 1 hr and incubated overnight separately with 1:1000 mouse primary anti-mouse MFN2 (Abcam ab56889) or 1:10000 anti-mouse actin (Sigma A2228). After washing, membranes were incubated for 1 hour with donkey anti-mouse or anti-rabbit secondary antibodies (LI-COR Biosciences) at 1:5-10,000 dilutions. Immunoblots were visualized on an Odyssey LI-COR Imaging System.

### 2.5 μCT analysis

Femurs from 8, 18, and 30 week old mice were fixed in 10% neutral buffered formalin (Di Ruscio and Associates, Inc., Fenton, MO) for 24 hours, and then stored in 70% ethanol. Bones were scanned by μCT40 (Scanco, Brüttisellen, Switzerland). For cancellous parameters, settings were 55 kVp, 10 μm resolution, lower threshold of 220, upper threshold of 1000, Gauss sigma of 0.4 and Gauss support of 1, with regions of interest selected proximal to the growth plate extending 200 slices. Cortical scans encompassed 100 slices at the mid-shaft at 55 kVp, 10 μm resolution, lower threshold of 260, upper threshold of 1000, Gauss sigma of 0.8 and Gauss support of 1.

### 2.5 Histomorphometric analysis

18 week-old mice were injected with calcein (10mg/kg) and alizarin red (30 mg/kg) seven and two days prior to sacrifice. Femurs were fixed in 10% neutral buffered formalin overnight, washed with PBS, incubated in 30% sucrose, embedded in OCT and sectioned longitudinally at 10 μm, using the Kawamoto method of tape transfer [17]. Unstained slides were imaged at 20x-resolution using Nanozoomer 2.0 HT whole slide scanner (Hamamatsu Photonics, Japan) with FITC/TRITC filters. Analysis of endocortical bone formation parameters was conducted by a blinded observer using BIOQUANT OSTEO software (v18.2.6, Bioquant Image Analysis Corp., Nashville, TN, USA).

### 2.6 P1NP and CTX

Serum was collected from 8 and 18 week old female mice, fasted overnight, via mandibular bleed (BD Microcontainer), and stored at −80°C. RatLaps P1NP and CTX-1 EIA assays (Immunodiagnostic Systems, Gaithersburg, MD, USA; AC-33F1 and AC-06F1, respectively) were conducted according to the manufacturer's instructions.

### 2.7 3-point bending

Isolated femurs from 8 week old male and female mice were used to assess bone strength by 3-point bending, as previously described [18]. Each femur was placed on supports 7 mm apart, and a transverse force applied until failure.

### 2.8 Mechanical loading

18 week old female mice were used to determine the force-strain relationship for tibial compression (n=6/genotype). The tibias were loaded to a peak force of −2N, −4N, −6N, and −8N with 2-3 minutes rest between each, and the strain recorded (FLK-1-11-1LJC, Tokyo Measuring Instruments Laboratory, Tokyo, Japan). 6N was needed to generate a peak compressive strain of −2200με in both WT and cKO mice. For mechanical loading, 18 week old WT and cKO females (n= 15 each) were anesthetized with 2% isofluorane and right tibias subjected to 1 bout per day for five days of cyclic axial compression using Electropulse 1000 (Instron, Norwood, MA, USA) at 4Hz, for 60 cycles at 6N. Calcein was injected intraperitoneally on the last day of loading, and alizarin red 5 days later, with sacrifice 7 days after the last loading bout [19]. Loaded (right) tibias or contralateral nonloaded control (left) tibias were embedded in methylmethacrylate and sectioned transversely at a distance 5 mm proximal to the distal tibiofibular junction to assess the area of peak strain, at 100 μm thickness. Images of a 30 μm depth were captured with a Leica DMi8 automated inverted microscope equipped with a TCS SPEII confocal module and max projection images were analyzed by a blinded observer using BIOQUANT OSTEO, as above, over the entire periosteal surface. For samples with no double-labeled surface, a value of 0.1 was imputed for MAR [20].

### 2.9 Oxygen consumption rate (OCR) and lactate measurement

Oxygen consumption rate (OCR) was studied according to the standard protocol provided by the manufacturer of the XF24 analyser (Agilent Seahorse, Agilent Technologies, Sana Clara, CA, USA) using XF96 cell culture microplates. For MSCs, cells were seeded at 65,000 cells per well overnight in αMEM 10% FBS prior to measurement. For days 3 and 7, MSCs were seeded at 50,000 and 25,000 respectively in growth medium. Cells were changed into OSM with 5 mM β-GP the following day and every 48 hours thereafter. The mitochondrial stress test used Oligomycin (1μM), carbonylcyanide *p*-(trifluoromethoxy) phenylhydrazone (FFCP, 0.5μM), and rotenone and antimycin A (each at 1μM). Upon completion of the assay, cells were scraped in 50μl RIPA buffer and protein concentration of each well was measured by BCA assay. OCR values are expressed as pmol/min/μg of total protein.

For lactate measurement, cells from 3 MFN2-cKO and 3 WT mice were seeded at 20,000 cells per well in 96 well-plates in 0.2 ml αMEM 10% FBS and cultured overnight. Subsequently, OSM (with 5 mM β-GP) was replaced every other day up to 13 days. Serial lactate levels were assessed according to the manufacturer instructions using L-Lacate assay kit (Eon Biosciences, 120001100A), using a 1:4 dilution of conditioned media, reading plates at $A_{490}$. Three technical replicates were averaged for each biological replicate. Immediately after media harvest, resazurin sodium (same compound as Alamar blue) (Thermo-Fisher, R12204 ) was added with fresh OSM and plates were read 6 hours later (Ex/Em 530/590), after which wells were gently rinsed and replenished with OSM without resazurin. The average of technical replicates for the L-lactate assay was normalized to the average of technical replicates for resazurin read on the day of media harvest. Relative cell number from the resazurin assay was shown by normalizing values of each biological replicate to its own reading at day 1, obtained prior to first addition of OSM.

### 2.10 Confocal Microscopy and Aspect Ratio Determination

MSCs (1.45 x $10^5$) were cultured in a 35mm glass bottom dish (Cellvis, Mountain View, CA) for 3 days. For loading with intracellular markers, cells were placed in a minimal amount of HBSS and incubated with 300 nM Mitotracker Green FM and 50 nm Lysotracker Red DND-99 (Thermo Fisher Scientific, Waltham, MA) for a period of 30 minutes. Following incubation, cells were washed two times with HBSS media, and were allowed to recover for 15 minutes. Imaging was performed on an inverted Zeiss LSM 880 confocal (Carl Zeiss, Jena, Germany) with cells placed at 37°C and 5% $CO_2$ in a Pelco PM S1 microscope stage-top incubation system. Mitotracker and lysotracker dyes were excited using 488 nm and 561 nm laser lines respectively, and imaged with a 63x/1.4 NA oil immersion objective. To minimize photobleaching, singlet oxygen formation was inhibited by the addition of 10 μM (±)-6-Hydroxy-2,5,7,8-tetramethylchromane-2-carboxylic acid (Trolox; Millipore Sigma, Burlington MA) to the imaging media. Images were acquired using the Airyscan detector operating in the 'Fast' mode functionally using a 186.7 nm Z-step pitch. For each culture, 5 distinct mitochondria from each of 6 confocally imaged cells were used to assess the aspect ratio (mitochondrial length/width) using the line tool in Image J.

### 2.11 Statistical analysis

Data is presented as mean ± SD with sample number indicated in each figure or legend. Statistical analysis was carried out using GraphPad Prism 8 (GraphPad, LaJolla, CA, USA) using two-way ANOVA with Sidak's multiple comparisons, or two-tailed unpaired t-tests with Welch's corrections when variances are unequal.

## Results

### 3.1 Loss of Mfn2 in the osteoblast lineage modestly increases cortical bone in 8 week old female mice

To determine how mitochondrial dynamics impacts osteogenesis *in vivo*, we generated *Mfn2* conditional knockout animals ($Mfn2^{fl/fl}$; $Prx\text{-}cre^{+/-}$ = cKO) and Cre-negative littermate controls ($Mfn2^{fl/fl}$; $Prx\text{-}cre^{-/-}$ = WT) by crossing male Mfn2 heterozygous Prx-Cre-positive males ($Mfn2^{fl/+}$; $Prx\text{-}cre^{+/-}$) with *Mfn2* floxed ($Mfn2^{fl/fl}$; $Prx\text{-}cre^{-/-}$) females. cKO mice showed no gross phenotype, including body weights (Supp Fig 1A). Depletion of Mfn2 mRNA was also confirmed in crushed bones (Suppl Fig 1B), while Mfn1 mRNA was unchanged (Suppl Fig 1C). We harvested femurs from both sexes at 8 weeks of age and performed *ex vivo* μCT. In males, there were no differences in any trabecular or cortical bone parameters between cKO and WT mice (Supp. Table 1). However, female cKO animals had a mild but significantly elevated cortical thickness (Ct.Th.) compared to WT littermates (Fig 1 A), although other parameters including trabecular bone volume fraction (BV/TV) were not substantially changed (Fig 1 B, Supp Table 2). At this age, neither serum P1NP, a marker of bone formation, nor CTX-1, a marker of resorption, was different by genotype in females (Fig 1C–D). Bone quality was assessed by a three-point bending test. In either sex, measures of maximum load, post-yield displacement, work to fracture, and stiffness were unchanged between WT and cKO groups (Supp Fig. 2).

### 3.2 MFN2 depletion enhances cortical bone thickness in 18 and 30 week old female mice

Since depletion of MFN2 had a mild effect on cortical bone mass in 8 week old female mice, we aged animals further. At 18 weeks, femurs of female mice analyzed by *ex vivo* microCT revealed a persistent increase in Ct.Th., but no significant differences in trabecular parameters between cKO mice compared to WT (Fig. 2 A–B, Supp. Table 2). Consistent with a thicker cortex, serum P1NP was elevated in female cKOs compared to WTs, whereas serum CTX levels were unaffected (Fig 2 C–D). Again, male mice showed no differences (Supp. Table 1). The phenotype of female mice at 30 weeks was similar to 18 weeks, with increased cortical thickness but not trabecular bone volume fraction (Supp. Table 2).

Given the persistent increase in cortical thickness from 8 to 30 weeks, we performed dynamic histomorphometry to assess OB activity on the endocortical surface using 18 week old female mice. While mineral apposition rate (MAR) was unchanged between cKOs and WTs, heightened mineralizing surface per bone surface (MS/BS) and bone formation rate (BFR/BS) in cKO females indicates that loss of MFN2 enhances bone mass by increasing the number of OBs, but not their individual bone-forming capacity in basal conditions (Fig 3 A–D). To further probe these cortical differences, we next challenged these mice with a mechanical anabolic stimulus. Tibias of 18 week old female mice were subjected to 5 days of cyclic compression, and contralateral nonloaded tibias served as controls. Surprisingly, the periosteal response to loading was similar in both genotypes (Supp. Fig. 3).

### 3.3 Osteogenesis is stimulated in MFN2-deficient cultures

To further explore the role of MFN2 in the OB, we expanded MSCs from WT and cKO bone marrow. *Mfn2* expression in WT MSCs increases during OB differentiation (Fig 4 A). MFN2 is depleted in cKO cells both at the RNA and protein level (Fig 4 A–B). As in the crushed bones, Mfn1 levels were not increased in compensation (Fig 4C). Based on the histomorphometric data at baseline, we suspected we might observe greater osteogenesis in MSCs isolated from cKO mice at low rather than high levels of stimulation. Concordantly, although differentiation was equivalent using the typical 10 mM concentration of β-GP (Supp Fig. 4), in a suboptimal dose (5 mM) the cKO cultures showed enhanced osteogenesis, with increased Alizarin Red staining (Fig 4 D,E) and upregulation of OB differentiation markers *Osx, Alp, Opn*, and *Ocn* (Fig 4 F–K).

### 3.4 Increased oxygen consumption and lactate production occurs in osteogenic cultures lacking MFN2

Others have shown that osteogenic induction of primary murine MSCs and the pre-osteoblast MC3T3 cell line is accompanied by robust increases in oxygen consumption at early stages of osteogenesis, while the late stage of OB differentiation is associated with increased glycolysis [1, 2, 21]. Therefore, we assessed basal and ATP-linked respiration and maximal oxygen consumption by Seahorse analysis in undifferentiated MSCs one day after replating, as well as with 3 or 7 days in low dose (5 mM) β-GP. Compared to WT cells, cKOs have consistently higher basal respiration, ATP linked respiration, and maximum respiratory capacity at all timepoints assessed (Fig 5 A–C, and Supp. Fig 5). MFN2 depletion does not affect mitochondrial mass, as mitochondrial DNA content is identical between groups during *in vitro* osteogenesis (Fig 5 D). However, as expected, loss of MFN2

changes mitochondrial morphology towards a more rounded shape that manifests as a decreased aspect ratio (Fig 5 E,F).

High levels of glycolysis late in OB differentiation *in vitro* are associated with release of lactate, which acidifies the culture media. Osteogenic cKO cultures consistently acidify their low dose OSM (day 12 and beyond), indicated by a change in medium color from pink to yellow, an effect not seen under the same conditions in WT cultures (Fig 5 G). Congruently, assessment of L-lactate in media collected over the 48 hour period between feedings indicates higher levels in cKO than WT (Fig 5 H). Interestingly, this occurred even at days 5-7, when overall oxygen consumption is decreasing from the peak at day 3, as well as at days 11-13 when mineralization is occurring. Thus, in MFN2-deficient cultures, accelerated OB differentiation is associated with both increased oxygen consumption and increased glycolysis.

## 3. Discussion

The metabolism of OBs is complex, with studies indicating that both aerobic glycolysis and oxidative phosphorylation are important for bone formation [1, 12, 22–24]. One way cells control the balance of these metabolic processes is via the morphology of the mitochondrial network, which is modulated by proteins such as MFN2. We generated mice with conditional deletion of *Mfn2* prior to osteolineage differentiation with Prx-Cre, finding a basal increase in cortical bone mass in female cKO mice at 8, 18, and 30 weeks of age compared to WT littermate controls. Intriguingly, this difference between genotypes did not persist under conditions of stimulated bone formation due to mechanical loading. While dynamic histomorphometry in basal conditions indicated greater OB numbers but not bone formation per cell, neither the number of active OBs nor bone formation per cell was increased in the cKO mice under loading conditions, Results from *in vitro* differentiation of marrow-derived MSCs also showed a greater effect of MFN2-depletion with a weak osteogenic stimulus but not a strong one. This concordance between the *in vivo* and *in vitro* findings suggests that the primary role of MFN2 in the OB may be to establish a higher threshold stimulus for differentiation. We propose that, with strong stimuli, there is no difference in response by MFN2 status because the threshold is met either way. On the other hand, MFN2 may play a role in the OB response to low mechanical loads, reducing bone formation that is not “needed” under these conditions.

Across many tissues, mitochondrial functions, including oxidative capacity, oxidative stress, and calcium regulation, show sex differences that impact pathologies, more frequently to a greater degree in females [25]. With respect to MFN2, its deletion in osteoclast lineage cells and brown adipose tissue both showed sex differences in phenotype. In the osteoclast-specific cKO mice, bone loss with age or RANKL stimulation was reduced only in female mice [26]. Loss of MFN2 in brown fat increased cold sensitivity in both male and female mice, but by different mechanisms [27]. Females with MFN2 loss in brown fat had increased oxygen consumption, due to increased fatty acid oxidation, while males increased glycolysis via PKM2. Inhibition of fatty acid oxidation in murine OBs, via deletion of the enzyme CPT2 [28], had a bigger effect on bone mass in females than males. Further work will be required to determine whether the female-specific bone phenotype in our MFN2-deficient

mice is caused by sex-dependent utilization of substrates such as glucose and fatty acids in OBs, or by another mechanism.

Previous work in most cell types suggests that reductions in MFN2 reduce oxidative phosphorylation [10]. However, we found that, despite abnormal mitochondrial morphology, cKO cultures displayed increased oxygen consumption early in osteogenesis, associated with enhanced osteogenic differentiation. In a study specifically addressing OB differentiation [29], Shares et al. found that increases in oxidative phosphorylation stabilized β-catenin via acetylation, thereby promoting osteogenesis, representing one possible mechanism by which MFN2 effects are directly related to mitochondrial energetics. However, it is now clear that mitochondria impact many cellular events, and MFN2 is a multifunctional protein involved in several signaling pathways associated with osteogenesis. In cancer cells, MFN2 has been shown to inhibit mTORC2 signaling via direct binding to Rictor [30]. Since mTORC2 plays a positive role in bone formation [31, 32], loss of MFN2 could increase this osteogenic signal. MFN2 has also been placed in the NOTCH pathway in T cells and cardiomyocytes [33, 34]. NOTCH is a suppressor of osteogenesis [35], so loss of MFN2 in this pathway could also promote differentiation. In multiple cell types, loss of MFN2 alters intracellular calcium levels and limits store-operated calcium entry [26, 36], likely due to its role in mitochondrial-endoplasmic reticulum interactions. In OBs, store-operated calcium entry seems to promote bone formation [37–39]. Interestingly, expression of a constitutively active form of STIM1 that elevates this calcium entry has differential effects on cortical and cancellous compartments; cortical bone was decreased while cancellous bone was increased in homozygous mutant mice [39]. Here, we found effects of MFN2 depletion only in cortical bone. Thus, abnormalities in calcium signals may also contribute to our MFN2-deficient phenotype in bone.

Another feature of MFN2 loss in our cKO system was an accelerated switch to aerobic glycolysis under osteogenic conditions, *in vitro*. Although this could represent a secondary effect of other aspects of differentiation, MFN2 has been implicated more directly in this process. In tumor cells, mTORC1 phosphorylates MFN2, enhancing its direct binding and inhibition of PKM2, a key enzyme in glycolysis, and loss of MFN2 promotes glycolysis [40]. Although the switch to glycolysis is important for bone formation [41], whether MFN2-PKM2 interactions play a role in this process in OBs is not known. If MFN2-PKM2 does modulate glycolysis in OBs, the effects are likely dependent on additional stage-dependent factors, since we observed the increase in glycolysis only after at least 12 days of osteogenesis.

One limitation of this study is that it used Prx-Cre, which is expressed early in development in all limb bud mesenchyme [15, 42], to drive deletion of *Mfn2*. Given the complexity of metabolic shifts during differentiation from uncommitted progenitors through osteoblastogenesis and active matrix secretion, it is possible that MFN2 plays distinct and potentially opposing roles at different points in the osteolineage. Further, although this Cre line has been used extensively to study bone, without mention of a Cre-only phenotype, we did not specifically compare WT Cre-positive and WT Cre-negative mice in our colony. Further work with other Cre drivers to manipulate MFN2 expression at more differentiated stages might be informative. We saw no secondary effect on bone resorption at either 8 or 18

weeks, indicated by normal serum CTX levels, making compensatory effects on OCs an unlikely source of the relatively modest phenotype observed. Loss of MFN2 in neutrophils and macrophages alters their response in inflammatory conditions [43, 44], and this study did not investigate bone formation in this context. Other studies indicate a potential role for MFN2 in osteoarthritis [45] and intervertebral disc degeneration [46], suggesting that the *Prx-cre;Mfn2*$^{fl/fl}$ mice generated here may show altered bone or cartilage responses to inflammatory stimuli.

In sum, we find that MFN2 in the osteolineage restrains bone formation, primarily at the level of OB differentiation. Interestingly, these in vivo effects occur only in the cortical compartment of female mice and not in males. OB progenitors lacking MFN2 show increased, rather than decreased, oxygen consumption early in differentiation, an effect that could reflect either intrinsic differences in mitochondrial function mediated by MFN2 or more rapid progression along the osteogenic pathway. Given the multitude of potential roles for MFN2 in cellular metabolism and the interactions between metabolism and OB differentiation, additional studies are needed to fully elucidate the mechanisms involved.

## Supplementary Material

Refer to Web version on PubMed Central for supplementary material.

## Acknowledgements

We thank Crystal Idleburg and Yung Kim for technical assistance and Dr. G. Mbalaviele for critical reading of the manuscript.

### Funding

This work was supported by NIAMS, National Institutes of Health Grants R01 AR052705 (to D. J. V.) and R01 AR070030 (to D. J. V. and R. F.) and R01 AR066551 (to R. F.), funding from Shriners Hospitals for Children (to D. J. V. and R. F.), as well as NIAMS, National Institutes of Health Metabolic Skeletal Disorders Training Program Grant T32AR060719 (to A. B.). Slide scanning was made possible with support from a Hope Center for Neurological Disorders shared instrumentation grant (NCRR, National Institutes of Health Grant 1S10RR027552) and μCT and histology by a Musculoskeletal Research Center grant (NIAMS, National Institutes of Health Grant P30 AR074992 (to R. F. and D. J. V.). POB and JAJF are supported by the Washington University Center for Cellular Imaging (WUCCI) which is funded in part by The Children's Discovery Institute of Washington University and St. Louis Children's Hospital (CDI-CORE-2015-505 and CDI-CORE-2019-813), the Foundation for Barnes-Jewish Hospital (3770 and 4642), the Washington University Rheumatic Diseases Research Resource-based Center (P30AR073752) and the Washington University Musculoskeletal Research Center (P30AR074992). The Zeiss LSM880 microscope used in the course of these studies was purchased with support from the Office of Research Infrastructure Programs (ORIP), a part of the NIH Office of the Director (S10OD021629).

The content is solely the responsibility of the authors and does not necessarily represent the official views of the National Institutes of Health.

## Abbreviations (in a footnote):

| | |
|---|---|
| **MFN** | Mitofusin |
| **cKO** | conditional knockout |
| **OB** | osteoblast |
| **MSC** | mesenchymal stromal cell |

| | |
|---|---|
| **β-GP** | β-glycerolphosphate |

## References


[1]. Guntur AR, Le PT, Farber CR, Rosen CJ, Bioenergetics during calvarial osteoblast differentiation reflect strain differences in bone mass, Endocrinology 155(5) (2014) 1589–95. [PubMed: 24437492]

[2]. Gao J, Feng Z, Wang X, Zeng M, Liu J, Han S, Xu J, Chen L, Cao K, Long J, Li Z, Shen W, Liu J, SIRT3/SOD2 maintains osteoblast differentiation and bone formation by regulating mitochondrial stress, Cell Death Differ. 25(2) (2018) 229–240. [PubMed: 28914882]

[3]. Guntur AR, Gerencser AA, Le PT, DeMambro VE, Bornstein SA, Mookerjee SA, Maridas DE, Clemmons DE, Brand MD, Rosen CJ, Osteoblast-like MC3T3-E1 Cells Prefer Glycolysis for ATP Production but Adipocyte-like 3T3-L1 Cells Prefer Oxidative Phosphorylation, J Bone Miner Res 33(6) (2018) 1052–1065. [PubMed: 29342317]

[4]. Canto C, Mitochondrial Dynamics: Shaping Metabolic Adaptation, International review of cell and molecular biology 340 (2018) 129–167. [PubMed: 30072090]

[5]. Liesa M, Shirihai OS, Mitochondrial dynamics in the regulation of nutrient utilization and energy expenditure, Cell Metab. 17(4) (2013) 491–506. [PubMed: 23562075]

[6]. Youle RJ, Narendra DP, Mechanisms of mitophagy, Nat. Rev. Mol. Cell. Biol 12(1) (2011) 9–14. [PubMed: 21179058]

[7]. Spinelli JB, Haigis MC, The multifaceted contributions of mitochondria to cellular metabolism, Nat Cell Biol 20(7) (2018) 745–754. [PubMed: 29950572]

[8]. Forni MF, Peloggia J, Trudeau K, Shirihai O, Kowaltowski AJ, Murine Mesenchymal Stem Cell Commitment to Differentiation Is Regulated by Mitochondrial Dynamics, Stem Cells 34(3) (2016) 743–55. [PubMed: 26638184]

[9]. Filadi R, Pendin D, Pizzo P, Mitofusin 2: from functions to disease, Cell death & disease 9(3) (2018) 330. [PubMed: 29491355]

[10]. Schrepfer E, Scorrano L, Mitofusins, from Mitochondria to Metabolism, Mol. Cell 61(5) (2016) 683–694. [PubMed: 26942673]

[11]. Li Q, Gao Z, Chen Y, Guan MX, The role of mitochondria in osteogenic, adipogenic and chondrogenic differentiation of mesenchymal stem cells, Protein & cell 8(6) (2017) 439–445. [PubMed: 28271444]

[12]. Chen CT, Shih YR, Kuo TK, Lee OK, Wei YH, Coordinated changes of mitochondrial biogenesis and antioxidant enzymes during osteogenic differentiation of human mesenchymal stem cells, Stem Cells 26(4) (2008) 960–8. [PubMed: 18218821]

[13]. Pietilä M, Palomäki S, Lehtonen S, Ritamo I, Valmu L, Nystedt J, Laitinen S, Leskelä HV, Sormunen R, Pesälä J, Nordström K, Vepsäläinen A, Lehenkari P, Mitochondrial function and energy metabolism in umbilical cord blood- and bone marrow-derived mesenchymal stem cells, Stem cells and development 21(4) (2012) 575–88. [PubMed: 21615273]

[14]. Sánchez-Aragó M, García-Bermúdez J, Martínez-Reyes I, Santacatterina F, Cuezva JM, Degradation of IF1 controls energy metabolism during osteogenic differentiation of stem cells, EMBO reports 14(7) (2013) 638–644. [PubMed: 23722655]

[15]. Logan M, Martin JF, Nagy A, Lobe C, Olson EN, Tabin CJ, Expression of Cre Recombinase in the developing mouse limb bud driven by a Prxl enhancer, Genesis (New York, N.Y. : 2000) 33(2) (2002) 77–80.

[16]. Chen H, McCaffery JM, Chan DC, Mitochondrial fusion protects against neurodegeneration in the cerebellum, Cell 130(3) (2007) 548–62. [PubMed: 17693261]

[17]. Kawamoto T, Use of a new adhesive film for the preparation of multi-purpose fresh-frozen sections from hard tissues, whole-animals, insects and plants, Arch. Histol. Cytol 66(2) (2003) 123–43. [PubMed: 12846553]

[18]. Willinghamm MD, Brodt MD, Lee KL, Stephens AL, Ye J, Silva MJ, Age-related changes in bone structure and strength in female and male BALB/c mice, Calcif. Tissue Int 86(6) (2010) 470–83. [PubMed: 20405109]

[19]. Sun D, Brodt MD, Zannit HM, Holguin N, Silva MJ, Evaluation of loading parameters for murine axial tibial loading: Stimulating cortical bone formation while reducing loading duration, J. Orthop. Res 36(2) (2018) 682–691. [PubMed: 28888055]

[20]. Dempster DW, Compston JE, Drezner MK, Glorieux FH, Kanis JA, Malluche H, Meunier PJ, Ott SM, Recker RR, Parfitt AM, Standardized nomenclature, symbols, and units for bone histomorphometry: a 2012 update of the report of the ASBMR Histomorphometry Nomenclature Committee, J Bone Miner Res 28(1) (2013) 2–17. [PubMed: 23197339]

[21]. Kawalec M, Boratynska-Jasinska A, Beresewicz M, Dymkowska D, Zablocki K, Zablocka B, Mitofusin 2 Deficiency Affects Energy Metabolism and Mitochondrial Biogenesis in MEF Cells, PLoS One 10(7) (2015) e0134162. [PubMed: 26230519]

[22]. Shum LC, White NS, Mills BN, Bentley KL, Eliseev RA, Energy Metabolism in Mesenchymal Stem Cells During Osteogenic Differentiation, Stem cells and development 25(2) (2016) 114–22. [PubMed: 26487485]

[23]. Esen E, Chen J, Karner CM, Okunade AL, Patterson BW, Long F, WNT-LRP5 signaling induces Warburg effect through mTORC2 activation during osteoblast differentiation, Cell Metab. 17(5) (2013) 745–55. [PubMed: 23623748]

[24]. Karner CM, Esen E, Chen J, Hsu FF, Turk J, Long F, Wnt Protein Signaling Reduces Nuclear Acetyl-CoA Levels to Suppress Gene Expression during Osteoblast Differentiation, J Biol Chem 291(25) (2016) 13028–39. [PubMed: 27129247]

[25]. Ventura-Clapier R, Moulin M, Piquereau J, Lemaire C, Mericskay M, Veksler V, Garnier A, Mitochondria: a central target for sex differences in pathologies, Clinical science (London, England : 1979) 131(9) (2017) 803–822.

[26]. Ballard A, Zeng R, Zarei A, Shao C, Cox L, Yan H, Franco A, Dorn GW 2nd, Faccio R, Veis DJ, The tethering function of mitofusin2 controls osteoclast differentiation by modulating the Ca2+-NFATC1 axis, J Biol Chem (2020).

[27]. Mahdaviani K, Benador IY, Su S, Gharakhanian RA, Stiles L, Trudeau KM, Cardamone M, Enriquez-Zarralanga V, Ritou E, Aprahamian T, Oliveira MF, Corkey BE, Perissi V, Liesa M, Shirihai OS, Mfn2 deletion in brown adipose tissue protects from insulin resistance and impairs thermogenesis, EMBO reports 18(7) (2017) 1123–1138. [PubMed: 28539390]

[28]. Kim SP, Li Z, Zoch ML, Frey JL, Bowman CE, Kushwaha P, Ryan KA, Goh BC, Scafidi S, Pickett JE, Faugere MC, Kershaw EE, Thorek DLJ, Clemens TL, Wolfgang MJ, Riddle RC, Fatty acid oxidation by the osteoblast is required for normal bone acquisition in a sex- and diet-dependent manner, JCI insight 2(16) (2017) e92704.

[29]. Shares BH, Busch M, White N, Shum L, Eliseev RA, Active mitochondria support osteogenic differentiation by stimulating beta-catenin acetylation, J Biol Chem 293(41) (2018) 16019–16027. [PubMed: 30150300]

[30]. Xu K, Chen G, Li X, Wu X, Chang Z, Xu J, Zhu Y, Yin P, Liang X, Dong L, MFN2 suppresses cancer progression through inhibition of mTORC2/Akt signaling, Scientific reports 7 (2017) 41718. [PubMed: 28176801]

[31]. Chen J, Holguin N, Shi Y, Silva MJ, Long F, mTORC2 signaling promotes skeletal growth and bone formation in mice, J Bone Miner Res 30(2) (2015) 369–78. [PubMed: 25196701]

[32]. Liu DM, Zhao L, Liu TT, Jiao PL, Zhao DD, Shih MS, Tao B, Sun LH, Zhao HY, Liu JM, Rictor/mTORC2 loss in osteoblasts impairs bone mass and strength, Bone 90 (2016) 50–8. [PubMed: 27262777]

[33]. Perumalsamy LR, Nagala M, Sarin A, Notch-activated signaling cascade interacts with mitochondrial remodeling proteins to regulate cell survival, Proc Natl Acad Sci U S A 107(15) (2010) 6882–7. [PubMed: 20339081]

[34]. Pei H, Du J, Song X, He L, Zhang Y, Li X, Qiu C, Zhang Y, Hou J, Feng J, Gao E, Li, Yang Y, Melatonin prevents adverse myocardial infarction remodeling via Notch1/Mfn2 pathway, Free Radic. Biol. Med. 97 (2016) 408–417. [PubMed: 27387769]

[35]. Hilton MJ, Tu X, Wu X, Bai S, Zhao H, Kobayashi T, Kronenberg HM, Teitelbaum SL, Ross FP, Kopan R, Long F, Notch signaling maintains bone marrow mesenchymal progenitors by suppressing osteoblast differentiation, Nat. Med. 14(3) (2008) 306–14. [PubMed: 18297083]

[36]. Kowaltowski AJ, Menezes-Filho SL, Assali EA, Goncalves IG, Cabral-Costa JV, Abreu P, Miller N, Nolasco P, Laurindo FRM, Bruni-Cardoso A, Shirihai OS, Mitochondrial morphology regulates organellar Ca(2+) uptake and changes cellular Ca(2+) homeostasis, FASEB J. 33(12) (2019) 13176–13188. [PubMed: 31480917]

[37]. Robinson LJ, Mancarella S, Songsawad D, Tourkova IL, Barnett JB, Gill DL, Soboloff J, Blair HC, Gene disruption of the calcium channel Orai1 results in inhibition of osteoclast and osteoblast differentiation and impairs skeletal development, Lab. Invest 92(7) (2012) 1071–83. [PubMed: 22546867]

[38]. Silva-Rojas R, Treves S, Jacobs H, Kessler P, Messaddeq N, Laporte J, Bohm J, STIM1 over-activation generates a multi-systemic phenotype affecting the skeletal muscle, spleen, eye, skin, bones and immune system in mice, Hum. Mol. Genet 28(10) (2019) 1579–1593. [PubMed: 30576443]

[39]. Gamage TH, Lengle E, Gunnes G, Pullisaar H, Holmgren A, Reseland JE, Merckoll E, Corti S, Mizobuchi M, Morales RJ, Tsiokas L, Tjønnfjord GE, Lacruz RS, Lyngstadaas SP, Misceo D, Frengen E, STIM1 R304W in mice causes subgingival hair growth and an increased fraction of trabecular bone, Cell Calcium 85 (2020) 102110. [PubMed: 31785581]

[40]. Li T, Han J, Jia L, Hu X, Chen L, Wang Y, PKM2 coordinates glycolysis with mitochondrial fusion and oxidative phosphorylation, Protein & cell 10(8) (2019) 583–594. [PubMed: 30887444]

[41]. Regan JN, Lim J, Shi Y, Joeng KS, Arbeit JM, Shohet RV, Long F, Up-regulation of glycolytic metabolism is required for HIF1alpha-driven bone formation, Proc Natl Acad Sci U S A 111(23) (2014) 8673–8. [PubMed: 24912186]

[42]. Logan MR, Lacy P, Odemuyiwa SO, Steward M, Davoine F, Kita H, Moqbel R, A critical role for vesicle-associated membrane protein-7 in exocytosis from human eosinophils and neutrophils, Allergy 61(6) (2006) 777–84. [PubMed: 16677249]

[43]. Zhou W, Hsu AY, Wang Y, Syahirah R, Wang T, Jeffries J, Wang X, Mohammad H, Seleem MN, Umulis D, Deng Q, Mitofusin 2 regulates neutrophil adhesive migration and the actin cytoskeleton, J. Cell Sci 133(17) (2020).

[44]. Tur J, Pereira-Lopes S, Vico T, Marin EA, Munoz JP, Hernandez-Alvarez M, Cardona PJ, Zorzano A, Lloberas J, Celada A, Mitofusin 2 in Macrophages Links Mitochondrial ROS Production, Cytokine Release, Phagocytosis, Autophagy, and Bactericidal Activity, Cell reports 32(8) (2020) 108079. [PubMed: 32846136]

[45]. Xu L, Wu Z, He Y, Chen Z, Xu K, Yu W, Fang W, Ma C, Moqbel SAA, Ran J, Xiong Y, Wu L, MFN2 contributes to metabolic disorders and inflammation in the aging of rat chondrocytes and osteoarthritis, Osteoarthritis Cartilage 28(8) (2020) 1079–1091. [PubMed: 32416221]

[46]. Chen Y, Lin J, Chen J, Huang C, Zhang Z, Wang J, Wang K, Wang X, Mfn2 is involved in intervertebral disc degeneration through autophagy modulation, Osteoarthritis Cartilage 28(3) (2020) 363–374. [PubMed: 31926268]

Author Manuscript

Author Manuscript

Author Manuscript

## Highlights

- Mitofusin2 limits cortical bone accrual in female mice
- Mitofusin2 is upregulated during early osteogenesis
- Despite disrupting mitochondrial networking in osteogenic cells, depletion of mitofusin2 increases oxygen consumption during early differentiation

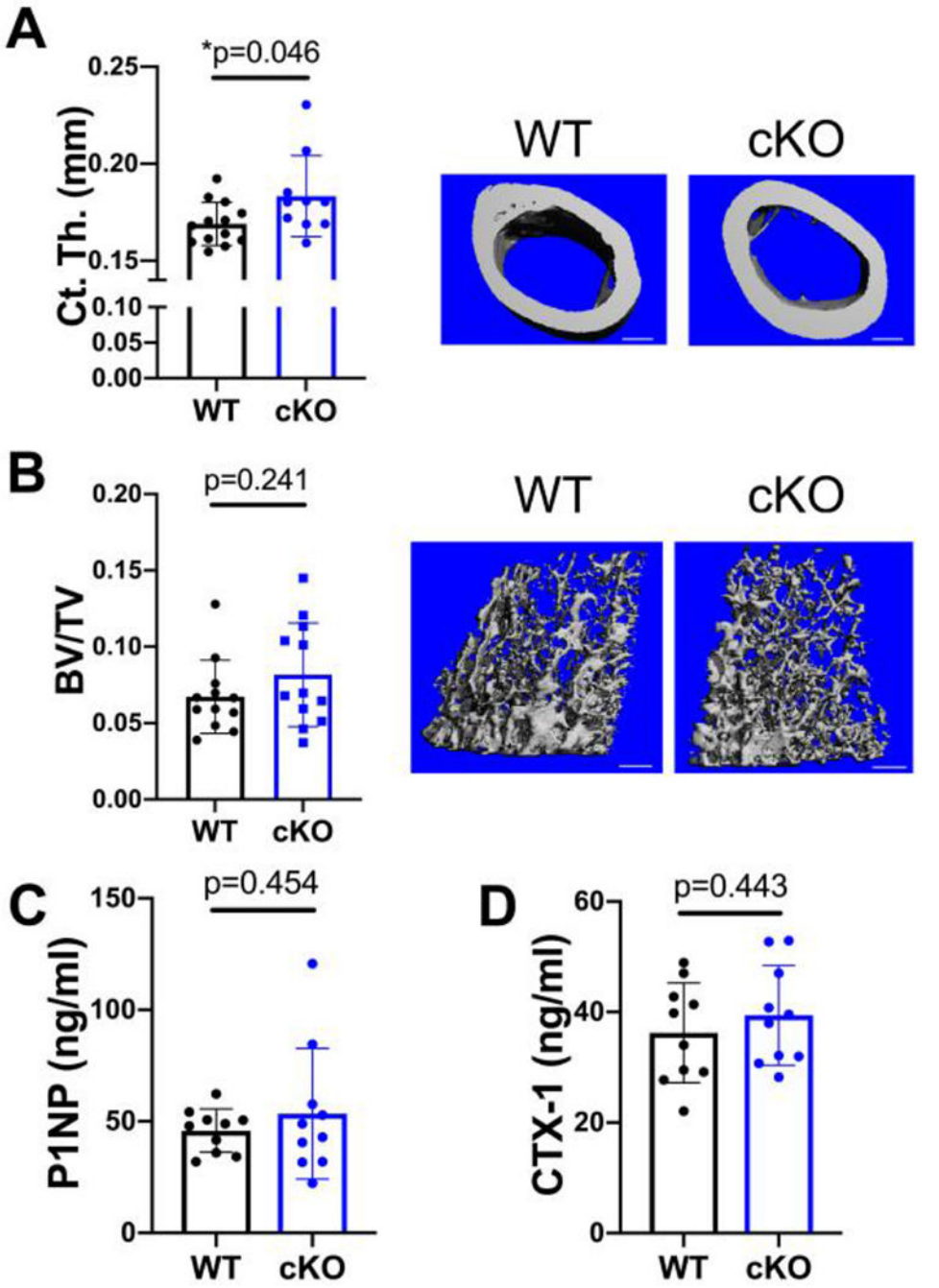


**Figure 1.**

Cortical bone is increased by MFN2 deficiency in the osteoblast lineage in growing females. A,B) MicroCT analysis shows that cortical thickness (Ct.Th, A), but not trabecular bone volume fraction (BV/TV, B) in the distal femur is increased at 8 weeks of age. Representative images shown with scale bars = 400 μm. C,D) Serum markers of bone turnover, P1NP (C) and CTX-1 (D), remain unchanged at this age. Unpaired t-tests shown, n=10.

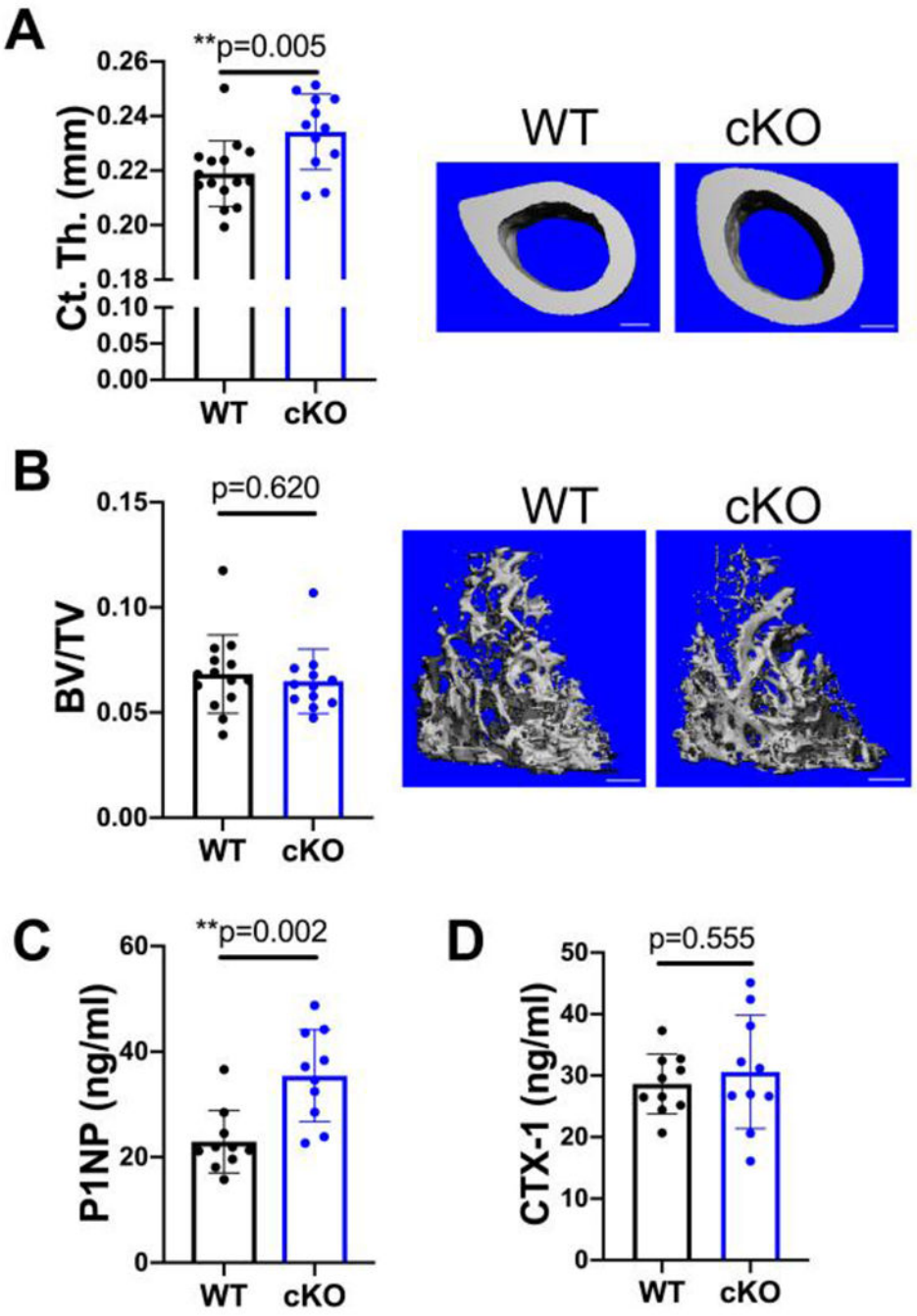


**Figure 2.**

Only cortical bone is increased by MFN2 deficiency at peak bone mass in females. A,B) MicroCT analysis of the distal femur shows that cortical thickness (Ct.Th A) is increased significantly while trabecular bone volume fraction is similar (BV/TV, B) at 18 weeks of age. Representative images with scale bars = 400 μm. C) The serum marker of bone formation, P1NP, is increased in MFN2 cKO 18 week females. D) CTX-1 remains unchanged at this age. Unpaired t-tests, n=10.

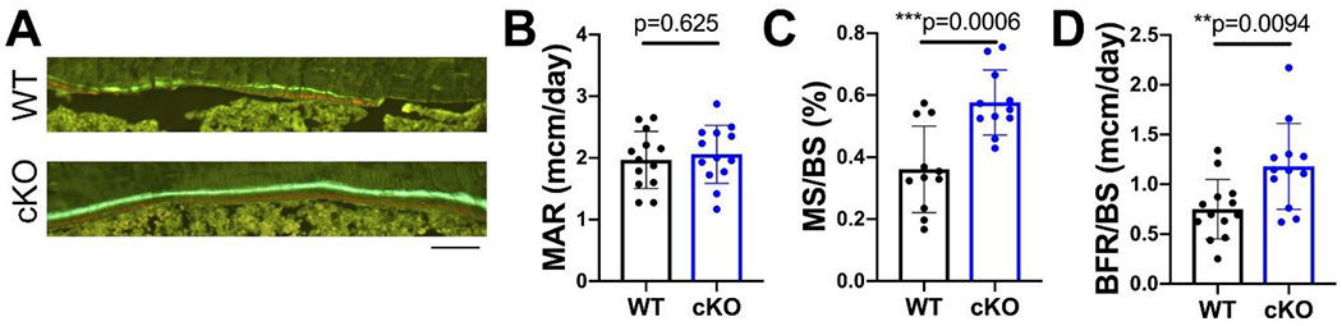


**Figure 3.**

Endocortical bone formation is increased in MFN2 cKO females. A) Representative images of alizarin red and calcein green labels along endocortical surface in 18 week old females. Scale bar = 100 μm. Dynamic histomorphometry along the endocortical surface in 18 week old female WT and cKO mice shows no change in mineral apposition rate (MAR, B), while mineralizing surface (MS/BS, C) and bone formation rate (BFR/BS, D) are increased. Unpaired t-tests with Welch's correction, n=12-13.

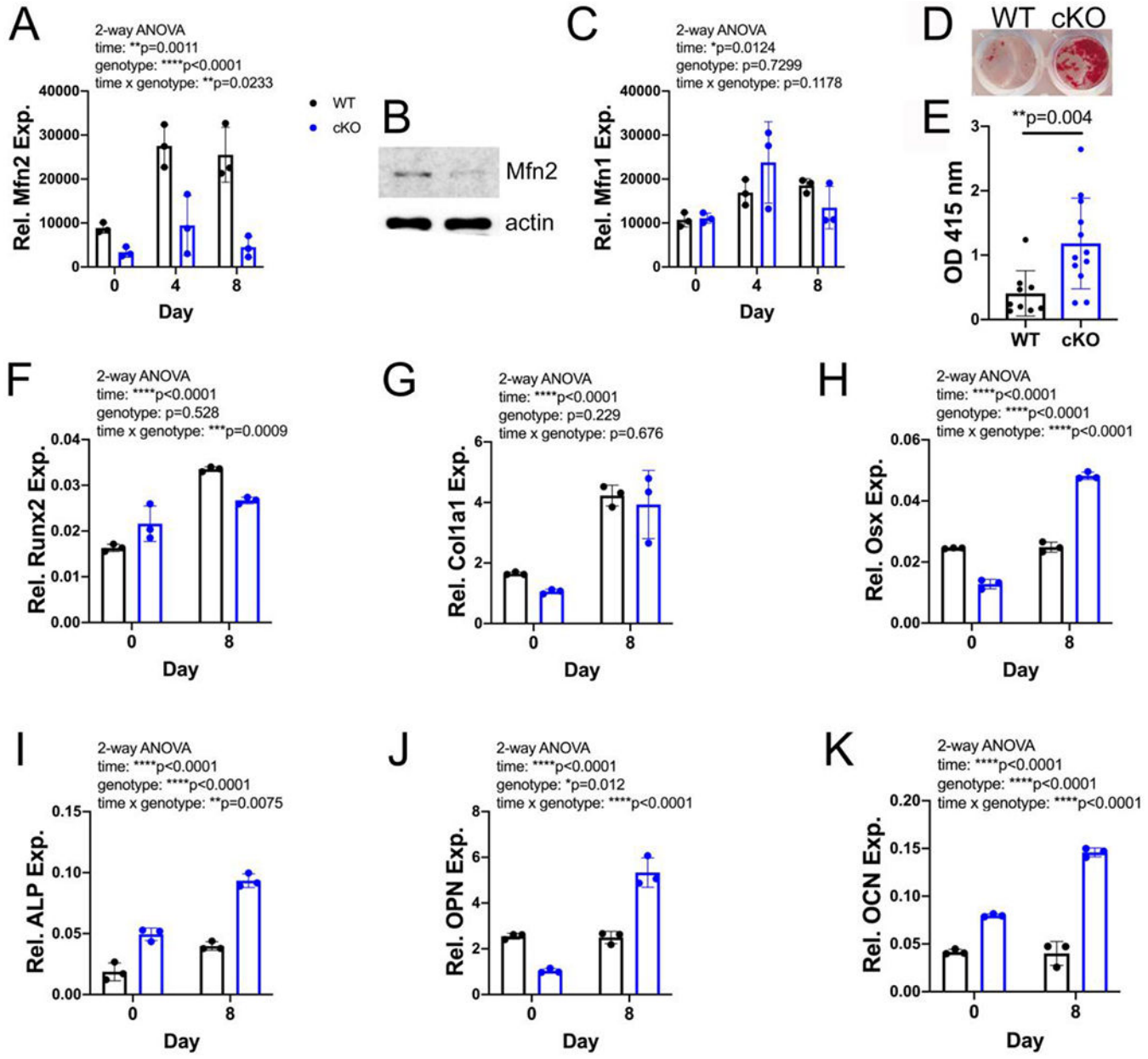


**Figure 4.**

In vitro osteogenesis is increased by MFN2 deficiency. A) Quantitative RT-PCR shows an increase in *Mfn2* mRNA during osteogenesis in vitro in WT but not cKO BMSCs. B) MFN2 protein is decreased in cKO MSCs. C) Mfn1 mRNA increases modestly during osteogenesis but is not different by genotype. D,E) cKO BMSC cultures stimulated with ascorbic acid and low dose (5 mM) β-GP show enhanced mineralization by alizarin red staining at day 16 (n=9-12 biological replicates). F-K) mRNA levels of many markers of osteogenesis increase more in cKO cultures differentiated in 5 mM β-GP for 8 days than in WT controls. Dots represent biological replicates, with WT in black and cKO in blue. 2-way ANOVA (A,C,J-K), t-test with Welch's correction (E).

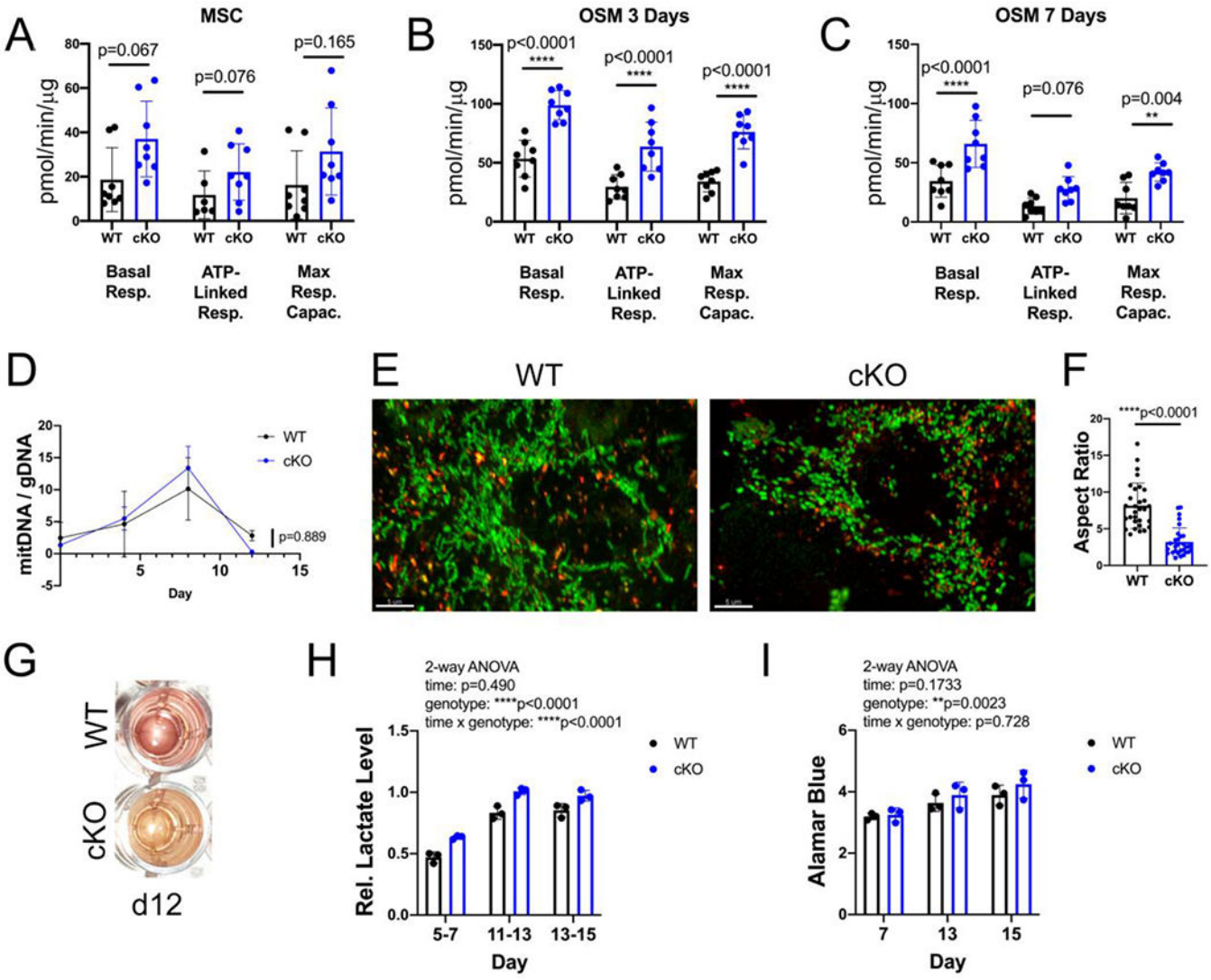


**Figure 5. Increased oxygen consumption despite abnormal mitochondrial morphology in early osteogenesis in MFN2- depleted cells.**

A-C) Oxygen consumption rates were measured in undifferentiated MSCs, or after 3 or 7 days of osteogenesis in 5 mM β–GP. Data are normalized to protein concentration of cell lysates extracted from each well, 4 technical replicates from 2 mice each genotype. D) Mitochondrial DNA copy number (mitDNA/gDNA) in MSCs at baseline, and differentiating in 10 mM osteogenic media over time. E) Mitochondrial morphology in MSCs, shown with Mitotracker green, and lack of co-localization with lysosomes, highlighted with Lysotracker red. Scale bar = 5 µm. F) Aspect ratio of mitochondria (length/width) is decreased in cKO MSCs. G) cKO cultures acidify their media during osteogenesis after 12 days, as seen by yellow color. H) Lactate, measured in media and normalized to cell number, is increased in cKO osteogenic cultures, measured in 3 biological replicates. I) Cell number during osteogenesis, from same plates as in H, does not differ between genotypes. Unpaired t-tests (A-C, F), 2-way repeated measures ANOVA (D, H, I).

## 2.12

Key Resources Table

| REAGENT or RESOURCE | SOURCE | IDENTIFIER |
|---|---|---|
| **Antibodies** | | |
| Anti-mouse MFN2 | Abcam | ab56889 RRID: AB_2142629 |
| Anti-mouse actin | Sigma | A2228 RRID: AB_476697 |
| IRDye 800CW Donkey anti-Mouse | LI-COR Biosciences | 926-32212 RRID: AB_2716622 |
| Anti-rabbit | LI-COR Biosciences | 926-32211 RRID: AB_621843 |
| **Chemicals, Peptides, and Recombinant Proteins** | | |
| MEM alpha medium | Gibco Life Technologies | A1049001 |
| β-glycerolphosphate disodium salt | Sigma | G9422 |
| L-Ascorbic acid 2-phosphate sesquimagnesium salt hydrate | Sigma | A8960 |
| RNA to cDNA EcoDry™ Premix | Takara Bio | 639549 |
| iTaq Universal SYBER Green Supermix | Bio-Rad | 1725121 |
| Halt™ Protease and Phosphatase Inhibitor Cocktail (100X) | ThermoFisher Scientific | 78442 |
| Nitrocellulose | Bio-Rad | 1620115 |
| 10% neutral buffered formalin | Di Russcio and Associates, Inc. | N/A |
| Calcein | Sigma | C0875 |
| Alizarin-30methyliminodiacetic acid | Sigma | A3882 |
| MitotrackerGreenFM | ThermoFisher Scientific | M7514 |
| LysotrackerRedDND-99 | ThermoFisher Scientific | L7528 |
| (±)-6-Hydroxy-2,5,7,8-tetramethylchromane-2-carboxylicacid | Trolox; MilliporeSigma | 238813 |
| **Critical Commercial Assays** | | |
| NucleoSpin RNA kit | Machery-Nagel | 740955.5 |
| DC Protein Assay | Bio-Rad | 5000116 |
| RatLaps P1NP assay | Immunodiagnostic Systems | AC-33F1 |
| CTX-1 EIA assay | Immunodiagnostic Systems | AC-06F1 |
| L-Lactate assay kit | Eon Biosciences | 120001100A |
| Resazurin Sodium Salt | Sigma | R7017 |
| **Oligonucleotides** | | |
| MFN2<br>F- 5'-AAGCACTTTGTCACTGCCAAG-3'<br>R- 5'-TTGTCCCAGAGCATGGCATTG-3' | Integrated DNA Technologies | N/A |
| MFN1<br>F-5'-TTGGCAGGACAAGTAGTGGC-3'<br>R-5'-AGCAGTTGGTTGTGTGACC-3' | | |
| ND1 (for mitochondrial DNA)<br>F- 5'-CCC ATT CGC GTT ATT CTT-3'<br>R-5'-AAG TTG ATC GTA ACG GAA GC-3' | Integrated DNA Technologies | N/A |
| LPL(for genomic DNA)<br>F- 5'-GGA TGG ACG GTA AGA GTG ATT C-3'<br>R- 5'-ATC CAA GGG TAG CAG ACA GGT-3' | Integrated DNA Technologies | N/A |

| REAGENT or RESOURCE | SOURCE | IDENTIFIER |
|---|---|---|
| PPIA/Cyclophillin A gDNA<br>F- 5'-AGCATACAGGTCCTGGCATC-3'<br>R- 5'-TTCACCTTCCCAAAGACCAC-3' | Integrated DNA Technologies | N/A |
| RUNX2<br>F- 5'-AACGATCTGAGATTTGTGGGC -3'<br>R- 5'-CCTGCGTGGGATTTCTTGGTT -3' | Integrated DNA Technologies | N/A |
| OSX<br>F- 5'-ATGGCGTCCTCTCTGCTTG -3'<br>R- 5'-TGAAAGGTCAGCGTATGGCTT -3' | Integrated DNA Technologies | N/A |
| COL1A1<br>F- 5'-AGACATGTTCAGCTTTGTGGAC-3'<br>R- 5'-GCAGCTGACTTCAGGGATG-3' | Integrated DNA Technologies | N/A |
| ALP<br>F- 5'-CCAACTCTTTTGTGCCAGAGA -3'<br>R- 5'-GGCTACATTGGTGTTGAGCTTTT -3' | Integrated DNA Technologies | N/A |
| OPN<br>F- 5'-AGCAAGAAACTCTTCCAAGCAA -3'<br>R- 5'-GTGAGATTCGTCAGATTCATCCG -3' | Integrated DNA Technologies | N/A |
| Cyclophilin<br>F- 5'-AGCATACAGGTCCTGGCATC-3'<br>R- 5'-TTCACCTTCCCAAAGACCAC-3' | Integrated DNA Technologies | N/A |
| Osteocalcin: QT00259406 1 Mm_Bglap_1_SG QuantiTect Primer Assay | QIAGEN LTD | Cat#QT00259406 |